

Biocompatibility of Gold Nanoparticles and Their Endocytic Fate Inside the Cellular Compartment: A Microscopic Overview

Ravi Shukla,[†] Vipul Bansal,[‡] Minakshi Chaudhary,[‡] Atanu Basu,[§]
Ramesh R. Bhonde,^{*,†} and Murali Sastry^{*,‡}

Tissue Engineering and Banking Laboratory, National Centre for Cell Science, Ganeshkhind, Pune 411 007, India, Nanoscience Group, Materials Chemistry Division, National Chemical Laboratory, Pune 411 008, India, and National Institute of Virology, 20 A, Dr. Ambedkar Road, Pune 411 001, India

Received May 23, 2005

Macrophages are one of the principal immune effector cells that play essential roles as secretory, phagocytic, and antigen-presenting cells in the immune system. In this study, we address the issue of cytotoxicity and immunogenic effects of gold nanoparticles on RAW264.7 macrophage cells. The cytotoxicity of gold nanoparticles has been correlated with a detailed study of their endocytic uptake using various microscopy tools such as atomic force microscopy (AFM), confocal-laser-scanning microscopy (CFLSM), and transmission electron microscopy (TEM). Our findings suggest that Au(0) nanoparticles are not cytotoxic, reduce the production of reactive oxygen and nitrite species, and do not elicit secretion of proinflammatory cytokines TNF- α and IL1- β , making them suitable candidates for nanomedicine. AFM measurements suggest that gold nanoparticles are internalized inside the cell via a mechanism involving pinocytosis, while CFLSM and TEM studies indicate their internalization in lysosomal bodies arranged in perinuclear fashion. Our studies thus underline the noncytotoxic, nonimmunogenic, and biocompatible properties of gold nanoparticles with the potential for application in nanoimmunology, nanomedicine, and nanobiotechnology.

Introduction

Nanomaterials are currently receiving considerable attention because of their potential applications in biology and medicine. Gold nanoparticles, which have interesting physicochemical properties,^{1,2} enjoy a long history dating back to Roman times and to the pioneering work of Faraday on the synthesis of stable aqueous dispersions of gold nanoparticles (gold hydrosols).³ It is of little surprise, therefore, that there are innumerable recipes in the literature for the synthesis of gold nanoparticles both in aqueous^{4–6} and organic solutions.^{7,8} In parallel with the development of new experimental processes for the synthesis of gold nanoparticles of controllable size, monodispersity, and shape, the chemistry related to surface modification of gold nanoparticles has also evinced considerable interest. The demonstration that amine^{9–11} and thiol¹² groups bind strongly to gold nanoparticles has

enabled surface modification of gold nanoparticles with amino acids^{13,14} and proteins,^{15,16} leading to important biomedical applications ranging from biodiagnostics,¹⁷ drug/DNA delivery,^{18,19} cell imaging,²⁰ immunostaining,²¹ and biosensing²² to electron microscopy markers.²³ The future use of gold nanoparticles in clinical applications is envisioned.²⁴

It is evident that, for any clinical application, biocompatibility of the nanoparticles is crucial. A key issue in evaluating their biocompatibility is assessing their potential cytotoxicity, either because of their size,²⁵ shape (e.g., needlelike carbon nanotubes^{26,27}), chemical composi-

* To whom correspondence should be addressed. E-mails: sastry@ems.ncl.res.in and rrbbhonde@nccs.res.in.

[†] National Centre for Cell Science.

[‡] National Chemical Laboratory.

[§] National Institute of Virology.

(1) Colvin, V. L.; Schlamp, M. C.; Alivisatos, A. P. *Nature* **1994**, 370, 354.

(2) Schmid, G., Ed.; *Clusters and Colloids*; VCH: Weinheim, Germany, 1994.

(3) Faraday, M. *Philos. Trans. R. Soc. London* **1857**, 147, 145.

(4) Turkevich, J.; Garton, G.; Stevenson, P. C. *J. Colloid Sci.* **1954**, 9, 26.

(5) Handley, D. A. *Colloidal Gold: Principles, Methods and Applications*; Hayat, M. A., Ed.; Academic Press: San Diego, CA, 1989; Vol. 1, chapter 2.

(6) Henglein, A. *Langmuir* **1999**, 15, 6738.

(7) Brust, M.; Walker, M.; Bethell, D.; Schiffrin, D. J.; Whyman, R. *J. Chem. Soc. Chem. Commun.* **1994**, 801.

(8) Selvakannan, P. R.; Mandal, S.; Pasricha, R.; Adyanthaya, S. D.; Sastry, M. *Chem. Commun.* **2002**, 13, 1334.

(9) Leff, D. V.; Brandt, L.; Heath, J. R. *Langmuir* **1996**, 12, 4723.

(10) Sastry, M.; Kumar, A.; Mukherjee, P. *Colloids Surf., A* **2001**, 181, 255.

(11) Selvakannan, P. R.; Mandal, S.; Phadtare, S.; Pasricha, R.; Sastry, M. *Langmuir* **2003**, 19, 3545.

(12) Templeton, A. C.; Wuelfing, W. P.; Murray, R. W. *Acc. Chem. Res.* **2000**, 33, 27.

(13) Selvakannan, P. R.; Mandal, S.; Phadtare, S.; Gole, A.; Pasricha, R.; Adyanthaya, S. D.; Sastry, M. *J. Colloid Interface Sci.* **2004**, 269, 97.

(14) Joshi, H.; Shirude, P. S.; Bansal, V.; Ganesh, K. N.; Sastry, M. *J. Phys. Chem. B* **2004**, 108, 11535.

(15) Gole, A.; Dash, C.; Soman, C.; Sainkar, S. R.; Rao, M.; Sastry, M. *Bioconjugate Chem.* **2001**, 12, 684.

(16) Phadtare, S.; Kumar, A.; Vinod, V. P.; Dash, C. V.; Rao, M.; Shukla, P. G.; Sivaram, S.; Sastry, M. *Chem. Mater.* **2003**, 15, 1944.

(17) Storhoff, J. J.; Mirkin, C. A. *Chem. Rev.* **1999**, 99, 1849.

(18) Niemeyer C. M. *Angew. Chem. Int. Ed.* **2001**, 40, 4128.

(19) Sanford, J. C.; Smith, F. D.; Russell, J. A. *Methods Enzymol.* **1993**, 217, 483.

(20) Bielinska, A.; Eichman, J. D.; Lee, I.; Baker, J. R., Jr.; Balogh, L. *J. Nanopart. Res.* **2002**, 4, 395.

(21) Roth, J. *Histochem. Cell Biol.* **1996**, 106, 1.

(22) Olofsson, L.; Rindzevicius, T.; Pfeiffer, I.; Kall, M.; Hook, F. *Langmuir* **2003**, 19, 10414.

(23) Baschong, W.; Wrigley, N. G. *J. Electron Microsc. Tech.* **1990**, 14, 313.

(24) Alivisatos, A. P. *Sci. Am.* **2001**, 285, 59.

(25) Service, R. F. *Science* **2000**, 290, 1526.

(26) Lam, C. W.; James, J. T.; McCluskey, R.; Hunter, R. L. *Toxicol. Sci.* **2004**, 77, 126.

(27) Warheit, D. B.; Laurence, B. R.; Reed, K. L.; Roach, D. H.; Reynolds, G. A. M.; Webb, T. R. *Toxicol. Sci.* **2004**, 77, 117.

tion (e.g., heavy metals^{28,29}), properties (e.g., carbon nanotubes that have reached the lungs are significantly more toxic than carbon black and graphite.^{26,27}) or because of the interaction of the nanoparticle surface with the cells (e.g., interaction of CdSe/ZnS particles with cells³⁰). Thus far, most cytotoxicity studies on nanomaterials have focused on aerosols³¹ and involve particle uptake by the lungs. Cytotoxic effects of heavy metals^{28,29} and quantum dots^{32,33} have been studied in detail. The toxicity of gold nanoparticles inside the biological system has always been an issue of concern. Despite the scientific literature available on cytotoxicity and immunotoxicology of gold(I)^{34–36} and gold(III)^{35–39} complexes and recent reports on cytotoxicity of cationic and anionic functionalized gold nanoparticles,⁴⁰ to our knowledge, little attention has been focused on the immunological response of cells to gold nanoparticles. Another issue that requires to be tackled prior to serious biomedical application of gold nanoparticles is that of the mode of internalization of the nanoparticles in the cells and their subsequent localization.

In this paper, we have focused on assessing whether aqueous gold nanoparticles [Au(0)] exert cytotoxicity on cells. More specifically, we have investigated the stress-induced and immunological response of RAW264.7 macrophages to gold nanoparticles. After ascertaining the noncytotoxicity of gold nanoparticles, we have carried out detailed microscopic analysis to delineate the pathway of particle uptake. Macrophage endocytosis of superparamagnetic iron oxide nanoparticles (which are already used in cellular biochemical pathways) has recently been shown.^{41a} To ascertain the endocytotic pathway of gold nanoparticles, we have used in this paper various microscopy techniques such as atomic force microscopy (AFM), confocal-laser-scanning microscopy (CFLSM), and transmission electron microscopy (TEM) to trace the time-dependent mechanism of gold nanoparticle uptake inside the macrophage cells. Our principal observations are that gold nanoparticles are inert and nontoxic to the cells as opposed to gold(I and III)-based antirheumatic drugs^{36,37} and that they do not elicit stress-induced secretion of proinflammatory cytokines such as TNF α and IL-1 β inside the macrophage cells. Moreover, at higher concentrations, gold nanoparticles inhibit the production of reactive

oxygen species (ROS) and reactive nitrite species (RNS), thereby indicating the versatile use of gold nanoparticle [Au(0)]-based systems in future clinical therapies and gold-based drug formulations. Our findings also suggest the pinocytotic uptake of gold nanoparticles by macrophage cells and their further localization in lysosomes, finally arranged in perinuclear fashion without entering the nucleus. Presented below are the details of the investigation.

Materials and Methods

Reagents and Materials. All chemicals and materials were obtained from Sigma-Aldrich Chemicals, St. Louis, MO, and used as-received unless otherwise mentioned.

Synthesis and Capping of Gold Nanoparticles. In a typical experiment, aqueous gold nanoparticles were synthesized by borohydride reduction of chloroauric acid (0.1 mM aqueous solution) in a manner similar to that described earlier.⁴² This procedure results in a ruby-red solution containing gold nanoparticles of diameter $35 \pm 7 \text{ \AA}$. The colloidal gold solution was dialyzed for 24 h in deionized water using dialysis membrane (molecular weight cut off 12 kDa) to remove excess free borohydride ions and un-reduced chloroaurate ions present in the solution, if any. The dialyzed gold nanoparticles were capped by lysine (lys)¹⁴ and poly-L-lysine (PLL) by addition of 5 mL of aqueous solutions of 1 mM lys and 0.05% PLL (molecular weight of ~ 4000), respectively, to 20 mL each of 0.1 mM dialyzed gold hydrosols. After addition of lys and PLL to the respective gold nanoparticle solutions and aging for 12 h, these solutions were again subjected to dialysis to remove uncoordinated lys and PLL molecules. The borohydride-reduced colloidal gold and lys- and PLL-capped colloidal gold solutions were concentrated by a factor of 2 by rotavapping at 72 mm and 50 °C to achieve a final gold nanoparticle concentration of 0.2 mM (assuming complete reduction of chloroaurate ions).

Synthesis of Fluorescent Gold Nanoparticles. Surface modification of the gold nanoparticles prepared as detailed above with fluorescein isothiocyanate (FITC) was achieved by addition of aliquots of aqueous solution of FITC to 0.2 mM colloidal gold solutions to achieve a final FITC concentration of 50 μM for emission spectroscopy and confocal microscopy studies. Variously functionalized gold nanoparticles were also capped with FITC to a final FITC concentration of 10 μM for additional emission studies. The solutions were allowed to equilibrate for 12 h under dark at 4 °C to avoid photo- and thermodeactivation of FITC molecules. Free FITC molecules, if any, in the colloidal gold solutions were removed by centrifugation at 6000 rpm for 20 min at 4 °C followed by two washings with deionized water, and the pellets containing FITC-bound gold nanoparticles were redispersed in deionized water and used for CFLSM. However, this low centrifugation speed was chosen to avoid the aggregation of gold nanoparticles at higher speed and thus avoiding the variation in the size of gold nanoparticles for CFLSM studies. The pellet obtained after centrifugation was redispersed in water such that the intensity of the nanogold solution obtained before and after centrifugation was the same.

UV-Vis Absorption Spectroscopy Studies. The binding of lys and PLL to the gold nanoparticles and their further binding to FITC was monitored by UV-vis spectroscopy on a Jasco dual-beam UV-vis-NIR spectrophotometer (model V-570) operated at a resolution of 2 nm.

Fluorescence Emission Spectroscopy Studies. Fluorescence spectroscopy is a powerful tool for studying the binding of fluorescent probes such as FITC to gold nanoparticles.⁴³ Quantitative analysis of FITC binding to pure Au, Au-lys, and Au-PLL nanoparticles was done using a Perkin-Elmer luminescence spectrophotometer (model LS 50B). Solutions containing FITC molecules were excited at 492 nm ($\lambda_{\text{ex}} = 492 \text{ nm}$), and the emission band was monitored in the range of 500–600 nm. Gold nanoparticle solutions having a final FITC concentration of 0.01 and 0.05 mM were prepared as described previously. The decrease

- (28) Goyer, R. A. *Am. J. Clin. Nutr.* **1995**, *61*, 646.
 (29) Sakurai, T.; Kaise, T.; Matsubara, C. *Chem. Res. Toxicol.* **1998**, *11*, 273.
 (30) Hoshino, A.; Fujioka, K.; Oku, T.; Suga, M.; Sasaki, Y. F.; Ohta, T.; Yasuhara, M.; Suzuki, K.; Yamamoto, K. *Nano Lett.* **2004**, *4*, 2163.
 (31) Videira, M. A.; Botelho, M. F.; Santos, A. C.; Gouveia, L. F.; Lima, J. J. P. D.; Almeida, A. J. *J. Drug Targeting* **2002**, *10*, 607.
 (32) Derfus, A. M.; Chan, W. C. W.; Bhatia, S. N. *Nano Lett.* **2004**, *4*, 11.
 (33) Kirchner, C.; Liedl, T.; Kudera, S.; Pellegrino, T.; Javier, A. M.; Gaub, H. E.; Stolzle, S.; Fertig, N.; Parak, W. J. *Nano Lett.* **2005**, *5*, 331.
 (34) Grootveld, M.; Blake, D. R.; Sahinoglu, T.; Claxton, A. W.; Mapp, P.; Stevens, C.; Allen, R. E.; Furst, A. *Free Radical Res. Commun.* **1990**, *10*, 199.
 (35) Gleichmann, E.; Kubicka-Muranyi, M.; Kind, P.; Goldermann, R.; Goerz, G.; Merk, H.; Rau R. *Rheumatol. Int.* **1991**, *11*, 219.
 (36) Grem, P.; Gleichmann, E. *Z. Rheumatol.* **1996**, *55*, 348.
 (37) Mirabelli, C. K.; Johnson, R. K.; Sung, C. M.; Fauchette, L. F.; Muirhead, K.; Crooke, S. T. *Cancer Res.* **1985**, *45*, 32.
 (38) Cossu, R.; Matovic, Z.; Radanovic, C.; Ponticelli, G. *Farmaco* **1994**, *49*, 301.
 (39) Svensson, A.; Moller, H.; Bjorkner, B.; Bruze, M.; Leden, I.; Theander, J.; Ohlsson, K.; Linder, C. *BMC Dermatol.* **2002**, *2*, 2.
 (40) (a) Goodman, C. M.; McCusker, C. D.; Yilmaz, T.; Rotello, V. M. *Bioconjugate Chem.* **2004**, *15*, 897. (b) Connor, E. E.; Mwamuka, J.; Gole, A.; Murphy, C. J.; Wyatt, M. D. *Small* **2005**, *1*, 325. (c) Bhattacharya, R.; Mukherjee, P.; Xiong, Z.; Atala, A.; Soker, S.; Mukhopadhyay, D. *Nano Lett.* **2004**, *4*, 2479.
 (41) (a) Raynal, I.; Prigent, P.; Peyramaure, S.; Najid, A.; Rebuzzi, C.; Carot, C. *Invest. Radiol.* **2004**, *39*, 56. (b) Chen, M.; von Mikecz, A. *Exp. Cell Res.* **2005**, *305*, 51.

- (42) Patil, V.; Malvankar, R. B.; Sastry, M. *Langmuir* **1999**, *15*, 8197.
 (43) Makarova, O. V.; Ostafin, A. E.; Miyoshi, H.; Norris, J. R., Jr. *J. Phys. Chem. B* **1999**, *103*, 9080.

in fluorescence intensity in the supernatants after centrifugation of FITC-bound gold nanoparticles is proportional to the FITC bound to the various gold nanoparticles.

TEM Measurements. Samples were prepared by drop-coating films of the different gold nanoparticle solutions on carbon-coated copper TEM grids followed by measurements on a JEOL model 1200EX instrument operated at an accelerating voltage of 120 kV.

Cell Culture. RAW264.7 macrophage cells were purchased from American Type Culture Collection (ATCC, Rockville, MD) and were cultured in Dulbecco's modified Eagle's medium (DMEM). The medium was supplemented with 10% fetal bovine serum (Gibco BRL, Carlsbad, CA), 100 units/mL penicillin, 100 μ g/mL streptomycin, and 2 mM glutamine in a humidified atmosphere of 5% CO₂ and 95% air at 37 °C.

Gold Nanoparticle Treatment and Cytotoxicity Determination by MTT Assay. Actively growing RAW264.7 cells were seeded at a density of 1×10^5 cells/well of a 96-well tissue culture plate (Falcon, BD Biosciences, Franklin Lakes, NJ) and incubated overnight. The cells were treated with different concentrations (10, 25, 50, and 100 μ M) of borohydride-reduced dialyzed gold nanoparticles for different times (24, 48, and 72 h) in quadruplets. Control cells were used without gold nanoparticle treatment. At the end of each exposure, the toxicity level of gold nanoparticles was assessed by 3-(4,5-dimethylazol-2-yl)-2,5-diphenyl-tetrazolium bromide (MTT) assay.⁴⁴ The MTT assay helps in cell-viability assessment by measuring the enzymatic reduction of yellow tetrazolium MTT to a purple formazan, as measured at 570 nm using SpectraMax 250 UV-vis microplate reader (Molecular Devices, Sunnyvale, CA). All experiments were performed 3 times in quadruplets, and the average of all of the experiments has been shown as cell-viability percentage in comparison with the control experiment, while gold untreated controls were considered as 100% viable.

Reactive Nitric Oxide Species (RNS) Determination. Nitrite (NO₂⁻) content was used as an index of nitric oxide (NO) production. Nitrite levels in supernatants of gold nanoparticle-treated cells after 24 and 48 h exposure were determined spectrophotometrically with the Griess reagent. A total of 50 μ L of the samples was added to 50 μ L of freshly prepared Griess reagent in a 96-well plate, and the absorbance was recorded at 540 nm. Dose- and time-dependent nitrite levels were plotted and compared to nanoparticle untreated control cells. RNS estimation was performed 3 times in quadruplets, and the average of all of the experiments has been shown along with the standard deviation bars.

ROS Determination by Flow Cytometry. Intracellular ROS was detected using flow cytometry as described by Bass and co-workers.⁴⁵ Briefly, a stock solution of DCFH-DA (50 mM) was prepared in methanol and stored at -20 °C in the dark. RAW264.7 macrophage cells were exposed to various concentrations of gold nanoparticles for 24 and 48 h. The green fluorescence of DCF was recorded by exciting the solutions with 488 nm argon laser (FL1) using a FACS Vantage system (Becton-Dickinson, San Jose, CA), and 10 000 events were counted per sample. FACS experiments were performed 3 times in quadruplets, and the representative FACS data has been shown. Also, the average of the mean fluorescent intensity of all of the experiments has been shown along with the standard deviation bars.

Semiquantitative Reverse Transcription Polymerase Chain Reaction (RT-PCR). RAW264.7 cells were seeded at a density of 5×10^5 cells/well of 6-well culture plates and grown overnight. The cells were treated with different concentrations of gold nanoparticles for 3 h. Bacterial lipopolysaccharide (LPS) (100 nM) treated cells served as a positive control, and untreated cells served as a standard control for RT-PCR analysis. The total RNA was extracted from controls and gold nanoparticle-treated RAW264.7 cells using the Trizol method (Life Technologies). For cDNA synthesis, 2 μ g of total RNA from each sample was incubated with a random primer, 0.1 μ M dithiothreitol (DTT), 500 μ M dNTPs, 40 units of RNase inhibitor, and 200 units of

Table 1

TNF- α	forward 5'-GCG AGG TGG AAC TGG CAG AAG-3' reverse 5'-GGT ACA ACC CAT CGG CTG GCA-3'
β actin	forward 5'-TGG AAT CCT GTG GCA TCC A-3' reverse 5'-TAA CAG TCC GCC TAG AAG CA-3'
IL-1 β	forward 5'-TCA TGG GAT GAT GAT AAC CTG CT-3' reverse 5'-CCC ATA CTT TAG GAA GAC ACG GAT T-3'

MMLV-reverse transcriptase (Life Technologies) for 1 h at 37 °C followed by incubation for 5 min at 95 °C. The transcripts from each sample were amplified from the cDNA using recombinant Taq polymerase (Life Technologies) under the following conditions: 95 °C for 2 min, 94 °C for 1 min, 68 °C for 1 min for TNF and 60 °C for 1 min for IL-1 β , and 72 °C for 1 min for a total of 30 cycles. β -Actin was used as a loading control. The primers used has been shown in Table 1.

Enzyme-Linked Immunosorbent Assay (ELISA). RAW264.7 cells were seeded at a density of 1×10^6 cells/well of 6-well culture plates and grown overnight. The cells were treated with different concentrations of gold nanoparticles for 24 h. Bacterial lipopolysaccharide (LPS) (100 nM) treated cells served as a positive control, and untreated cells served as a standard control. The culture supernatants were assayed for the proinflammatory cytokines TNF- α and IL-1 β by using Opt-EIA kits (BD Biosciences) according to the instructions of the manufacturer.

Effect of Gold Nanoparticles on Total Cell Proteins. Total cell proteins were isolated from actively growing RAW264.7 cells treated with or without 100 μ M concentrations of borohydride-reduced dialyzed gold nanoparticles for 24 h using RIPA lysis buffer (20 mM Tris at pH 7.5, 150 mM NaCl, 1% NP-40, 1% TritonX-100, 0.1% SDS, 1% sodium deoxycholate, and the protease inhibitor cocktail). Proteins were quantified by the Bradford method (BioRad, Hercules, CA), and 25 μ g of protein was resolved using 10% SDS-PAGE⁴⁶ and stained using Coomassie brilliant blue.

AFM Measurements. Cell imaging was done in the tapping and contact modes by AFM on a VEECO Digital Instruments multimode scanning probe microscope equipped with a NanoScope IV controller. For sample preparation, RAW264.7 macrophage cells were seeded at a density of 5×10^4 cells/mL per glass coverslip and grown for a period of 24 h. The cells were exposed to 50 μ M gold nanoparticles for 5 min followed by several washings with chilled PBS (pH 7.0). In another experiment, the cells were given a pulse of 50 μ M gold nanoparticles for 15 min followed by an overnight chase in media at 37 °C in humidified atmosphere containing 5% CO₂ and 95% air. The cells were fixed with freshly prepared 2% chilled paraformaldehyde (ICN, Aurora, OH) in PBS for 10 min. Paraformaldehyde, unlike glutaraldehyde, preserves the immunogenicity of the cell-surface proteins. After fixation, the cells were washed 5 times with chilled PBS (pH 7.0), and coverslips were attached to metallic packs with conducting double-sided tape. The metallic packs were mounted on a 6399e-piezoscanner (10 μ m) for AFM analysis. For tapping mode AFM, 125- μ m-long etched silicon probes and, for contact mode AFM, 100- μ m-long silicon nitride probes were used. Phase and friction images were collected in the tapping and contact mode, respectively, at a scanning frequency of 1 Hz.

CFLSM. RAW264.7 cells were seeded at a density of 5×10^4 cells/mL per glass coverslip and grown for a period of 24 h. The cells were exposed to 50 μ M FITC-coupled gold nanoparticle solutions for different time periods followed by several washings with chilled PBS (pH 7.0). In some experiments, the cells were also treated with lysotracker dye (Molecular Probes) for 30 min as per the protocol of the supplier. The cells were fixed with freshly prepared 3.7% chilled paraformaldehyde (ICN, Aurora, OH) for 10 min, washed with chilled PBS (pH 7.0), and mounted with antifade 1,4-diazobicyclo-2,2,2-octanex (DABCO) in mounting medium. The coverslips were observed under the confocal

(44) Mosmann, T. *J. Immunol. Methods* **1983**, *65*, 55.

(45) Bass, D. A.; Parce, J. W.; Dechatelet, L. R.; Szejda, P.; Thomas, M. C. S. *J. Immunol.* **1983**, *130*, 1910.

(46) Laemmli, U. K. *Nature* **1970**, *227*, 680.

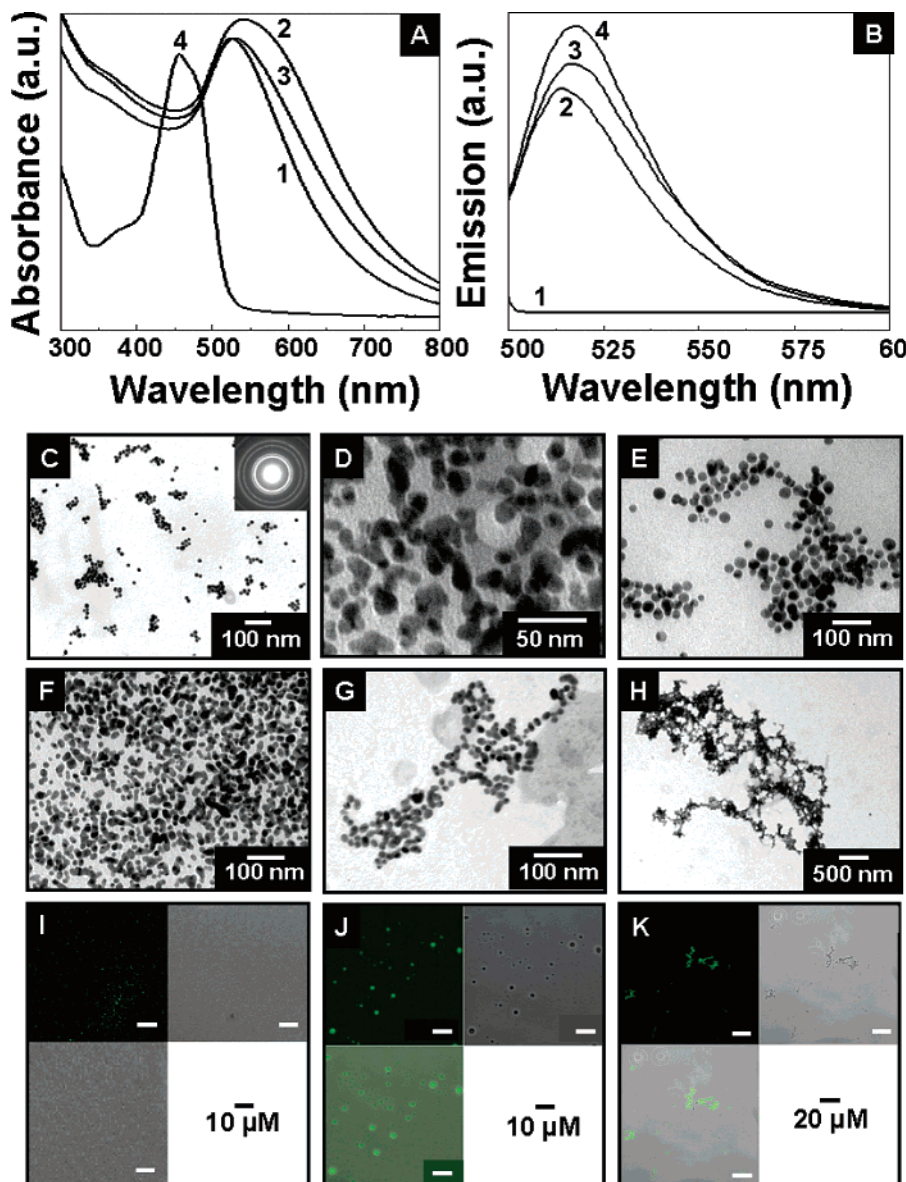


Figure 1. Physicochemical characterization of gold nanoparticles by (A) UV-vis absorption spectroscopy, (B) fluorescence emission spectroscopy, (C–H) transmission electron microscopy, and (I–K) confocal laser scanning microscopy. Curves 1–4 in A and B correspond to borohydride-reduced gold nanoparticles (curve 1), Au-lys (curve 2), Au-PLL (curve 3), and FITC (curve 4). Curves in B correspond to fluorescence emission spectra derived from the supernatants obtained after centrifugation of respective colloidal gold solutions using $10 \mu\text{M}$ FITC. C–H show TEM images obtained from borohydride-reduced gold (C), Au-lys (D), Au-PLL (E), Au-FITC (F), Au-lys-FITC (G), and Au-PLL-FITC (H). The inset in C shows the selected area electron diffraction pattern obtained from the gold nanoparticles. I–K show CFLSM images obtained from solutions corresponding to those in F–H, respectively.

laser-scanning microscope (Carl Zeiss, Germany) fitted with a CCD-4230 camera, using computer-based programmable image analyzer KS300 (Carl Zeiss, Germany).

TEM Studies on the Cells. RAW264.7 macrophage cells were seeded at a density of 1×10^6 cells in a 60 mm tissue culture dish and grown overnight. The cells were treated with $50 \mu\text{M}$ gold nanoparticles for 24 h. The cells were washed thoroughly with chilled PBS, pelleted by centrifugation, and fixed with 0.1% glutaraldehyde. Cell cryotomy was performed, and images were recorded at 100 kV using a Tecnai 12 Biotwin TEM (FEI, Eindhoven, The Netherlands).

Results and Discussion

Physicochemical Characterization of Gold Nanoparticles. UV-vis spectra of the dialyzed borohydride-reduced gold hydrosol, lysine (lys), and poly-L-lysine (PLL) capped gold hydrosols and FITC (curves 1–4, respectively) are shown in Figure 1A. A strong absorption in curve 1 at ca. 527 nm is observed that corresponds to excitation

of surface plasmon vibrations in the gold nanoparticles. When the gold nanoparticles are capped with lys or PLL, a broadening and red shift of the surface plasmon band is observed (curves 2 and 3, respectively), which indicates surface complexation by the amino acid (lys) and peptide (PLL) and, hence, possibly some aggregation of the gold nanoparticles consequent to surface modification. Interestingly, the spectrum recorded from Au-lys nanoparticles (curve 2) shows a greater broadening and red shift in comparison with that of Au-PLL nanoparticles (curve 3). The interaction between aqueous gold nanoparticles with lys and PLL thus appears to be quite complex. The solution containing FITC molecules shows an absorption maximum at ca. 456 nm.

The solutions containing gold nanoparticles and lysine and PLL-capped gold nanoparticles were functionalized with fluorescein isothiocyanate (FITC), a fluorescent probe often used for cell imaging, and the relative binding of

FITC molecules to colloidal gold, Au-lys, and Au-PLL were studied. Figure 1B shows the fluorescence emission spectra recorded from the supernatants obtained from 10 μM FITC-functionalized gold nanoparticles (curve 1), Au-lys (curve 2), and Au-PLL (curve 3) after centrifugation and from free FITC at the same concentration (curve 4). The decrease in the emission intensity of the above-mentioned solutions in comparison with the FITC solution is a measure of the extent of binding of FITC molecules to the different gold nanoparticle solutions. It is evident from the curves that the uncapped gold nanoparticles (curve 1) show maximum binding of FITC followed by Au-lys (curve 2) and Au-PLL (curve 3), respectively. In fact, the uncapped gold nanoparticles are observed to bind almost all of the FITC molecules in the solution (curve 1), indicating the possibility that there might still be some additional sites available for FITC binding on the gold nanoparticle surface. To completely functionalize the surface of gold nanoparticles with FITC molecules, a higher concentration of FITC (final concentration of 50 μM) was used. Figure S1A in the Supporting Information shows the fluorescence emission spectra recorded from supernatants obtained from 50 μM FITC-functionalized gold nanoparticles (curve 1), Au-lys (curve 2), and Au-PLL (curve 3) after centrifugation and from free FITC in solution at the same concentration (curve 4). At higher concentrations of FITC, trends similar to those observed at lower concentrations of FITC (Figure 1B) are seen; i.e., uncapped gold nanoparticles (curve 1 in Figure S1A in the Supporting Information) showed more binding of FITC that is followed by Au-lys (curve 2 in Figure S1A in the Supporting Information) and Au-PLL (curve 3 in Figure S1A in the Supporting Information) in that order. However, at the higher FITC concentration of 50 μM , the gold nanoparticle surface is saturated with FITC molecules, as is evident by the increase in emission intensity because of fluorescence from free FITC molecules in the solution (compare curves 1 in Figure 1B and Figure S1A in the Supporting Information). The quantitative estimation of the amount of FITC bound to various gold nanoparticles was done by plotting a standard calibration curve (Figure S1B in the Supporting Information) using 2.5 μM (point 1), 5 μM (point 2), 12.5 μM (point 3), 25 μM (point 4), and 50 μM (point 5) FITC concentrations, followed by linear curve fitting. The concentration of free FITC in nanogold solutions shown in Figure S1A in the Supporting Information was calculated using this standard calibration curve, which in turn gives the concentration of FITC bound to various gold nanoparticles. The amount of FITC bound to 100 μM Au, Au-lys, and Au-PLL is found to be ca. 1.33, 1.06, and 0.16 μM , respectively. Because the isothiocyanate group of FITC is a strong nucleophile, which is known to form stable complexes with gold,³⁷ it is reasonable to expect that FITC binds to gold via the sulfur atom. Whereas, in the case of Au-lys and Au-PLL, because of nonavailability of the free gold surface for thiol linkage, electrostatic interaction between the amine and carboxylic groups of FITC and lys or PLL molecules on the surface of gold nanoparticles appears to be the major mode of linkage. The relatively higher concentration of FITC molecules bound to uncapped gold nanoparticles in comparison with Au-lys and Au-PLL nanoparticles can be explained on the basis of the fact that the FITC thiol–gold interactions are relatively stronger than amine–gold interactions.⁹ The higher binding of FITC molecules to Au-lys than Au-PLL can also be explained; the isothiocyanate moiety of FITC is well-known to bind to the ϵ -amine group and N-terminal α -amine group of lysine residues.⁴⁷ While lys contains two free amine groups (α and ϵ), in the PLL chain, the α -amine

group of each lys moiety is occupied in amide bond formation, except the N-terminal free α -amine group, and hence, only the ϵ -amine groups are free in PLL for binding. The presence of a larger number of free amine groups on the gold nanoparticle surface in the case of lys rather than PLL could explain the higher binding of FITC molecules to lys rather than PLL.

The above-mentioned functionalized gold nanoparticles were observed under TEM and CFLSM. The TEM images recorded from as-prepared borohydride-reduced gold nanoparticles and Au-lys and Au-PLL nanoparticles are shown in parts C–E of Figure 1, respectively. A comparison of the micrographs shows that, while the average morphology of the particles is spherical, gold nanoparticles of various functionalities show varying degrees of particle aggregation. The as-prepared borohydride-reduced gold particles are in close contact after water evaporation (Figure 1C) as is to be expected from the fact that they are not stabilized with an amino acid or a peptide. The Au-lys (Figure 1D) and Au-PLL (Figure 1E) nanoparticles appear to be assembled into open, string-like structures and would explain the broadening and shift in the surface plasmon band observed in the UV–vis measurements from these samples (Figure 1A). The extent of aggregation is maximum for Au-PLL (Figure 1E), suggesting a higher degree of interparticle hydrogen bonding in this case. Parts F–H of Figure 1 show TEM images recorded from the as-prepared borohydride-reduced gold nanoparticles and Au-lys and Au-PLL nanoparticles, respectively, after further functionalization with FITC molecules. All of these gold nanoparticle solutions functionalized with FITC show aggregation of gold nanoparticles as evident from the TEM images (parts F–H of Figure 1). A comparison of these images indicates a relatively higher degree of aggregation in Au-PLL–FITC than in Au-lys–FITC followed by the Au–FITC nanoconjugates. The FITC-conjugated Au-lys (Figure 1G) and Au-PLL (Figure 1H) nanoparticles also appear to be assembled into open, string-like structures of increasing lengths. These FITC-conjugated borohydride-reduced gold nanoparticles and Au-lys and Au-PLL nanoparticles were also observed under CFLSM, shown in parts I–K of Figure 1, respectively. As a control, FITC only, when seen under CFLSM, following the same washing steps as during sample preparation, did not result in any fluorescence under CFLSM. In the case of Au–FITC nanobioconjugates (Figure 1I), excited at 488 nm using an argon laser, even though we managed to observe fluorescence directly through the objective lens of the microscope, we could not adequately image the Au–FITC nanobioconjugates. This observation appears to be contrary to the fluorescence emission spectroscopy data (Figure 1B) in which the gold nanoparticles show good conjugation to fluorescent ligand FITC. This inability to image the FITC-capped gold nanoparticles by CFLSM indicates rapid quenching in fluorescence intensity from Au–FITC nanoparticles (Figure 1I). Quenching of the excited state by the conductive metal surface that results in energy transfer to the metal surface has been reported earlier.^{48,49} The probability of this Forster energy transfer depends upon the overlap of the fluorescence band of the dye molecule with the absorption band of the acceptor.⁴⁹ In the present case, the FITC fluorescence band at 518 nm (Figure 1B) overlaps with the gold surface plasmon

(47) Blakeslee, D.; Baines, M. G. *J. Immunol. Methods* **1976**, 13, 305.

(48) Drexhage, K. H.; Kuhn, H.; Shafer, F. P. *Ber. Bunsen-Ges. Phys. Chem.* **1968**, 72, 329.

(49) Dulkeith, E.; Morteani, A. C.; Niedereichholz, T.; Klar, T. A.; Feldmann, J.; Levi, S. A.; van Veggel, F. C. J. M.; Reinhoudt, D. N.; Moller, M.; Gittins, D. I. *Phys. Rev. Lett.* **2002**, 89, 203002.

band at 527 nm (Figure 1A), and one expects effective energy transfer from the excited molecule to the gold surface. Hence, addition of spacer groups between the gold nanoparticles and FITC molecules to avoid energy transfer might provide a useful strategy to avoid rapid quenching of fluorescence emission from FITC. Lys and PLL were used as spacer groups between the gold nanoparticles and FITC molecules because of the electrostatic and hydrogen-bonding considerations mentioned earlier. The Au-lys-FITC and Au-PLL-FITC nanobioconjugates, when excited by the 488 nm argon laser, showed considerably stable fluorescence, and excellent confocal microscopy images (parts J–K of Figure 1) could be routinely captured. The images recorded using CFLSM are in accordance with those observed by TEM and further confirms the formation of large string-like aggregates in the case of Au-PLL-FITC and to a lesser extent in Au-lys-FITC nanobioconjugates. For the above reasons, Au-lys-FITC nanobioconjugates were used in further confocal microscopy experiments.

Cytotoxicity of Gold Nanoparticles *in Vitro*. The cytotoxicity of gold nanoparticles under *in vitro* conditions in RAW264.7 macrophage cells was examined in terms of the effect of gold nanoparticles on cell proliferation by the MTT assay, production of reactive nitric oxide species (NOS) by the Griess reagent, and production of ROS by flow cytometry (fluorescence-activated cell sorting). To examine whether gold nanoparticles affect cell proliferation, the MTT assay (Figure 2A) was performed. Untreated cells as well as cells treated with 10, 25, 50, and 100 μ M concentrations of gold nanoparticles for 24, 48, and 72 h were subjected to the MTT assay for cell-viability determination. After 48 h of gold nanoparticles treatment, RAW264.7 macrophage cells showed more than 90% viability up to 100 μ M concentrations of gold nanoparticles (Figure 2A). Although after 72 h, there is a marginal decrease in cell viability to the 85% level for 100 μ M gold nanoparticle treatment. This slight decrease in the cell number might be accounted for by the stress caused to the cells because of depletion in media nutrients level as a result of the presence of cells in the same media continuously for 72 h. These results suggest that Au(0) nanoparticles do not show detectable cytotoxicity up to 100 μ M concentration of gold until 72 h of exposure, in contrast to the previous reports that have shown the cytotoxic nature of Au(I) and Au(III) gold complexes.^{36–38} Our results on noncytotoxicity of borohydride-reduced gold nanoparticles are in agreement with the conclusions of some recent studies on a range of surface-modified gold nanoparticle preparations.⁴⁰

To determine whether gold nanoparticles affect the production of reactive nitrite species (RNS) in the macrophage cells, RAW264.7 macrophage cells were treated with 10, 25, 50, and 100 μ M gold nanoparticles (blocks 1–4, respectively) for 24 and 48 h (Figure 2B). It is interesting to observe that, when treated with a 50 μ M colloidal gold solution, there is no change in the RNS level up to 24 h in comparison with the untreated control; however, after 100 μ M gold nanoparticle treatment, we observed a reduction in the cellular RNS level. On the other hand, when the effect of gold nanoparticles on the cellular RNS level was observed after 48 h of treatment, a concentration-dependent reduction in RNS levels was observed. These data suggest a time- and dose-dependent reduction of RNS levels on gold nanoparticle treatment.

The effect of gold nanoparticles on the production of ROS in macrophage cells was studied by flow cytometry using the fluorescence-activated cell sorter (FACS). RAW264.7 macrophage cells were treated with 10, 25, 50,

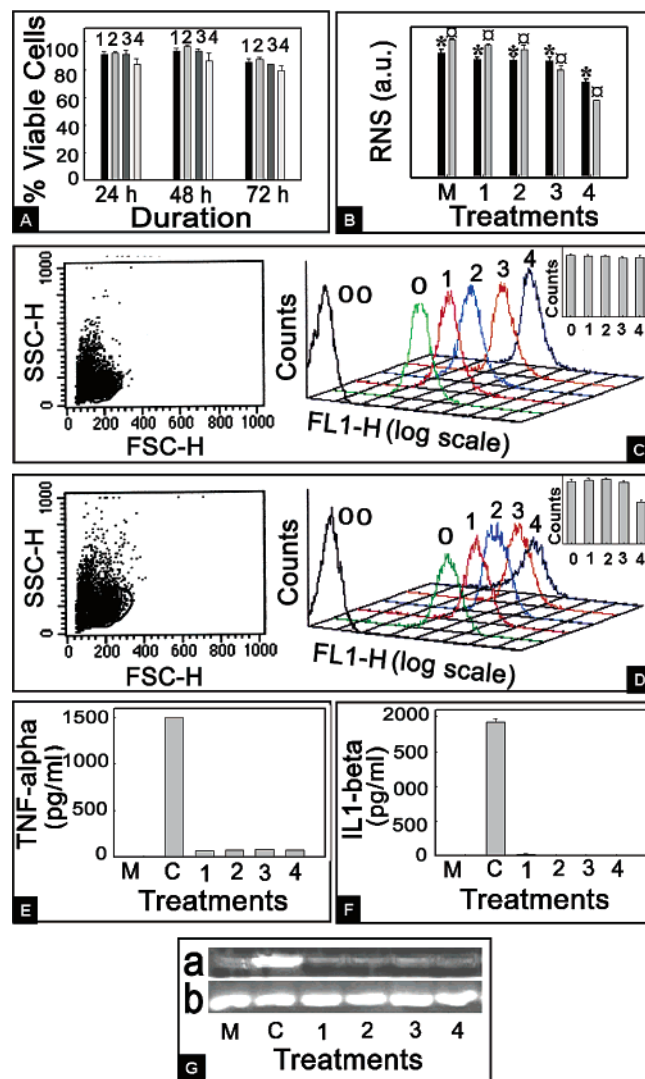


Figure 2. Cytotoxicity studies of gold nanoparticles on RAW264.7 macrophage cells. (A) MTT assay showing cell viability during exposure of cells to 10, 25, 50, and 100 μ M colloidal gold for 24, 48, and 72 h, respectively. (B) Reactive nitrite species (RNS) determination after 24 h (*) and 48 h (x) of 10, 25, 50, and 100 μ M gold nanoparticle treatment. (C and D) FACS data in plots on the left side showing forward and side FSC–SSC scatter plots obtained from cells before gold exposure and curves on right side showing fluorescence intensity height (FL1-H) as an estimate of ROS after 24 h (C) and 48 h (D) of 10, 25, 50, and 100 μ M gold nanoparticle treatment. (E and F) ELISA showing expression of TNF- α (E) and IL-1 β (F) after 24 h of gold nanoparticle treatment and (G) RT-PCR data showing production of TNF- α at an mRNA level after 3 h of gold nanoparticle treatment. In curves and plots, C, M, 00, 0, 1, 2, 3, and 4 correspond to LPS treatment (C), no treatment, i.e., media (M), unstained untreated cells (00), no gold nanoparticle treatment (0), 10 μ M (1), 25 μ M (2), 50 μ M (3), and 100 μ M (4) gold nanoparticle treatments, respectively.

and 100 μ M gold nanoparticles for 24 h (Figure 2C) and 48 h (Figure 2D), and forward and side scatter (FSC/SSC) plots (left panels in parts C and D of Figure 2) as well as fluorescence intensity (FL1-H) curves (right panels in parts C and D of Figure 2) were obtained. In the FSC/SSC plots of control cells as well as gold-treated cells after 24 h (left panel in Figure 2C) and 48 h (left panel in Figure 2C) of treatment, two different populations of cells were observed. With varying gold nanoparticle treatment, out of two cell populations, the population depicted on the left side in each scatter plot (FSC/SSC scatter plots in parts C and D of Figure 2) does not vary, and hence, the population

diverging with increasing gold nanoparticle treatment (cell population on the right side of FSC/SSC plots in parts C and D of Figure 2) was gated for creating FL1-H curves.

The right panels in parts C and D of Figure 2 show the FL1-H curves obtained from the gated populations in respective FSC/SSC plots after treating RAW264.7 macrophage cells with 10, 25, 50, and 100 μ M gold nanoparticles for 24 h (curves 1–4 in Figure 2C) and 48 h (curves 1–4 in Figure 2D), followed by cell staining using DCFH-DA, an ROS-specific fluorescent dye. Unstained cells not exposed to gold nanoparticles were taken as the fluorescence control (curve 00 in parts C and D of Figure 2), while stained, gold-untreated cells were taken as reaction control (curve 0 in parts C and D of Figure 2). It is clear from curves 0–4 in Figure 2C that there is no effect of different concentrations of gold nanoparticles (curves 1–4 in Figure 2C) on the ROS level in macrophage cells up to 24 h of treatment (Figure 2C) in comparison with that in untreated cells (curve 0 in Figure 2C). However, when treated up to 48 h (Figure 2D) with various amounts of gold nanoparticles (curves 1–4 in Figure 2D) and up to 50 μ M colloidal gold treatment (curves 1–3 in Figure 2D), the gold nanoparticles do not seem to effect ROS levels. On the other hand, exposure to 100 μ M concentration gold nanoparticles (curve 4 in Figure 2D) does lead to a reduction in the ROS level when compared with that in the control (curve 0 in Figure 2D). The insets in parts C and D of Figure 2 show the mean fluorescent intensity from the three experiments done in quadruplets along with the error bars, arising from the respective samples, indicating the statistical validity of the data, thus strengthening the dose- and time-dependent outcome of results.

The ROS data (parts C and D of Figure 2) correlate well with the RNS data (Figure 2B), which also show a reduction in RNS levels at higher gold concentrations after prolonged exposure. It has been shown that Au(I) compounds inhibit the DNA-binding activity of AP-1 and NF- κ B transcription factors, which in turn downregulate the expression of a number of genes viz. IL-2 receptors and proinflammatory cytokines that, in turn, would reduce the production of RNS and ROS.^{50a} The similar mechanism of downregulation of RNS and ROS might also be involved in Au(0) nanoparticles. Further experiments are in progress to show the exact mechanism of downregulation of these species in Au(0) nanoparticles. However, in contrast to Au(0) nanoparticles, the Au(III) compounds have been reported^{50b} to oxidize cellular self-proteins to convert them into modified-proteins, causing self-peptide molecules to elicit immune response and hence giving rise to autoimmune diseases. Hence, a time- and dose-dependent decrease in both RNS and ROS levels on Au(0) treatment indicates that gold nanoparticles exert, directly and/or indirectly, antioxidant effects on macrophages, which might eventually be helpful in treatment of various diseases including autoimmune diseases such as rheumatoid arthritis.

Macrophages are one of the principal immune effector cells and, hence, in addition to cytotoxicity studies, the immunological response of RAW264.7 macrophage cells when exposed to gold nanoparticles was studied in terms of the production of proinflammatory cytokines TNF- α and IL1- β , both at the mRNA (after 3 h) (Figure 2G) and protein (after 24 h) (parts E and F of Figure 2) level. Neither the control cells nor the cells treated with gold nanopar-

ticles up to 100 μ M concentration express mRNA for either TNF- α or IL1- β . Although TNF- α mRNA was detected in the cells treated with bacterial LPS (Figure 2G), we could not detect IL1- β mRNA even in the cells treated with bacterial LPS. This might be due to the fact that IL1- β mRNA is inducibly produced at a later stage in comparison with TNF- α mRNA, and in both of the cases, the mRNA used in this study was isolated after 3 h of incubation. To assess whether any additional effect of gold nanoparticles was exerted on the process of translation, particularly in the case of IL1- β where mRNA expression could not be obtained even in the case of the positive control (LPS), production of proinflammatory cytokines was tested at the protein level by ELISA (parts E and F of Figure 2). Neither TNF- α (Figure 2E) nor IL1- β (Figure 2F) were found to be expressed significantly after 24 h of incubation either in control cells (untreated) or in the cells treated with gold nanoparticles up to 100 μ M concentrations. However, cells stimulated with bacterial LPS expressed a significant amount of TNF- α (Figure 2E) or IL1- β (Figure 2F). Hence, the ELISA results obtained are in agreement with the RT-PCR results. These results suggest that gold nanoparticles do not elicit an initial immunological response and do not induce the production of proinflammatory cytokines TNF- α and IL1- β up to high gold nanoparticle doses of 100 μ M.

In addition to cytotoxicity and immunological studies, the effect of gold nanoparticles on the secretion of major cellular proteins involved in higher order cellular functions was also studied to find out whether gold nanoparticles cause any additional effects, particularly on the major biochemical pathways of the macrophage cells. The SDS-PAGE data of the protein profile of untreated RAW264.7 macrophage cells (lane 2) and of cells treated with 100 μ M gold nanoparticles for 24 h (lane 3) are shown in the Supporting Information (Figure S2). It is clear that there is no change in the profile of the major cellular proteins after gold nanoparticle treatment of macrophage cells up to 100 μ M gold concentration and, thus, little effect on the higher order cellular functions of macrophage cells.

Endocytotic Uptake of Gold Nanoparticles. Macrophages are known to internalize solutes very rapidly, taking in the equivalent of their cell volume every 2 h.⁵¹ It is therefore important to correlate any study on the cytotoxicity of gold nanoparticles with a detailed microscopy analysis about the pathway of particle uptake.³³ An understanding of the uptake of gold nanoparticles is also extremely important for drug- and gene-delivery applications. We have used AFM, CFLSM, and TEM to trace the time-dependent kinetics of gold nanoparticle uptake inside the macrophage cells.

AFM was used to study the initial stages of endocytosis. RAW264.7 macrophage cells were treated with a 50 μ M gold nanoparticle solution for different times as described in the Materials and Methods and were examined by tapping (Figure 3) and contact (Figure 4) mode AFM. Untreated cells were taken as a control.

Parts A and B of Figure 3 show the tapping mode height (1) and phase images (2) of the control cells without treatment with gold nanoparticles, respectively. The untreated cells clearly show a part of a well-defined nucleus (toward the left side of the images) along with some regions of the protruding cell membrane. The nucleus is clearly distinguishable from the cell membrane because of its greater height (lighter color signifies more height) than the cell membrane in the height image (panel 1 in

(50) (a) Kataoka, K.; Handa, H.; Nishizawa, M. *J. Biol. Chem.* **1999**, 276, 34074. (b) Isab, A. A.; Sadler, P. *J. Biochim. Biophys. Acta* **1977**, 492, 322.

(51) Steinman, R. M.; Brodie, S. E.; Cohn, J. A. *J. Cell Biol.* **1976**, 68, 665.

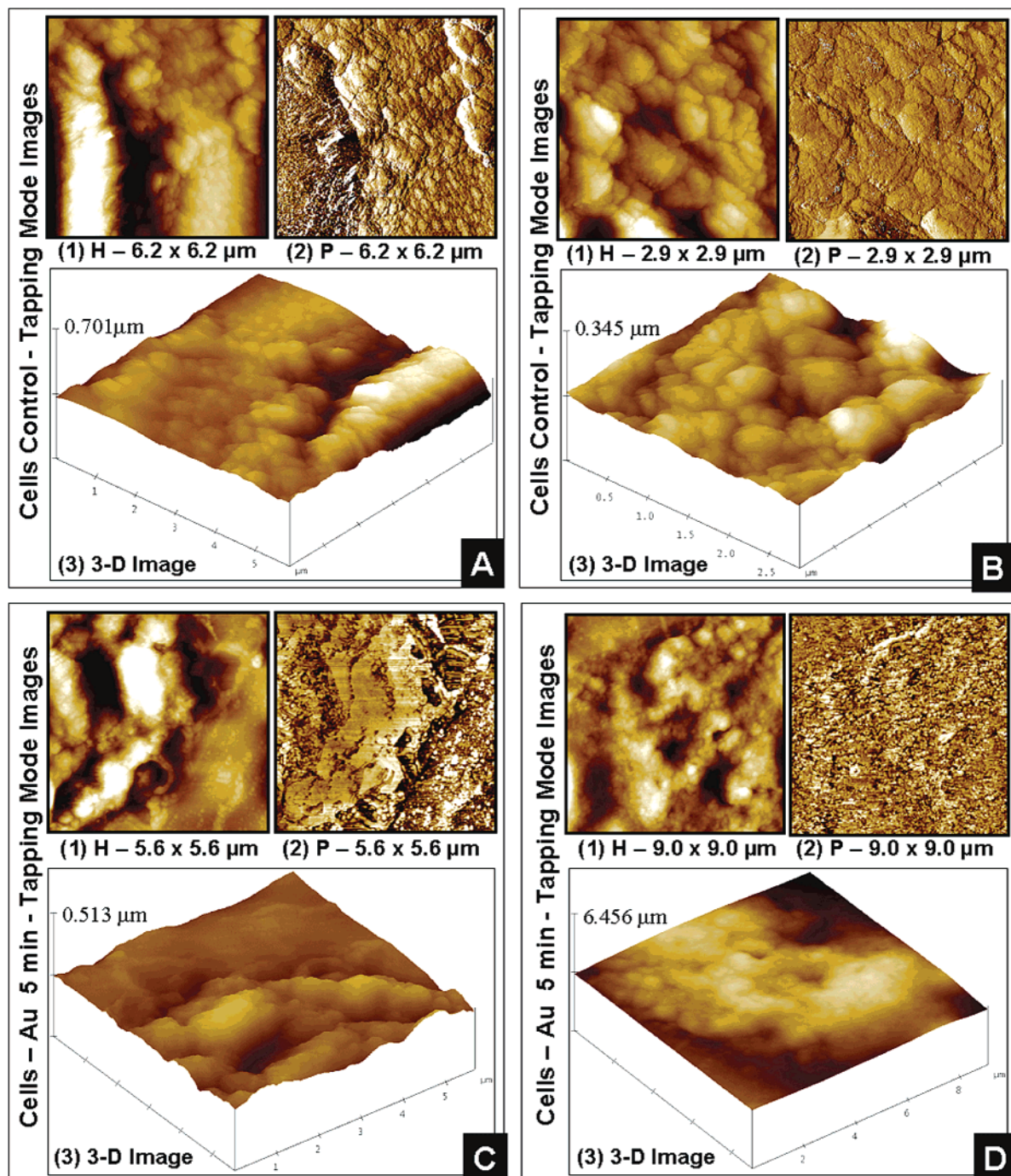


Figure 3. Tapping mode AFM images of RAW264.7 macrophage cells obtained before gold nanoparticle treatment (A and B) and after 5 min of gold exposure (C and D). The notations H and P correspond to height (image 1) and phase (image 2) images, respectively. Images 3 in A–D are the 3D images of the height images shown in the respective panels. All images were taken in air.

Figure 3A) and higher contrast than that of the cell membrane in the phase image (panel 2 in Figure 3). The 3D view (panel 3 in Figure 3A) of the height image further supports the information obtained in panels 1 and 2 in Figure 3A. The cell-membrane architecture (Figure 3B) is clearly visible in the higher magnification image of the membrane region of the cells.

Parts C and D of Figure 3 show the tapping mode height and phase images of the cells treated with 50 μ M gold nanoparticles for 5 min, again clearly exhibiting a part of the well-defined nucleus (toward the left side of the images of panels 1 and 2 in Figure 3C) along with some regions of the protruding cell membrane. The nucleus is clearly distinguishable here from the cell membrane in the height

image (panel 1 in Figure 3C), but in the phase image (panel 2 in Figure 3C), the cell membrane shows a higher contrast than the nucleus, suggesting the presence of higher contrast gold nanoparticles on the cell surface but not on the nucleus. The 3D view (panel 3 in Figure 3C) of the height image also clearly shows the presence of a well-defined nucleus. Figure 3D shows the region of the cell membrane in greater detail. The higher contrast of the cell-membrane region is clearly underlined in this image and is significantly higher than that of this region in the absence of gold nanoparticles (control in panel 2 in Figure 3B).

Parts A and B of Figure 4 show the contact mode height and friction images of the cells treated with 50 μ M gold

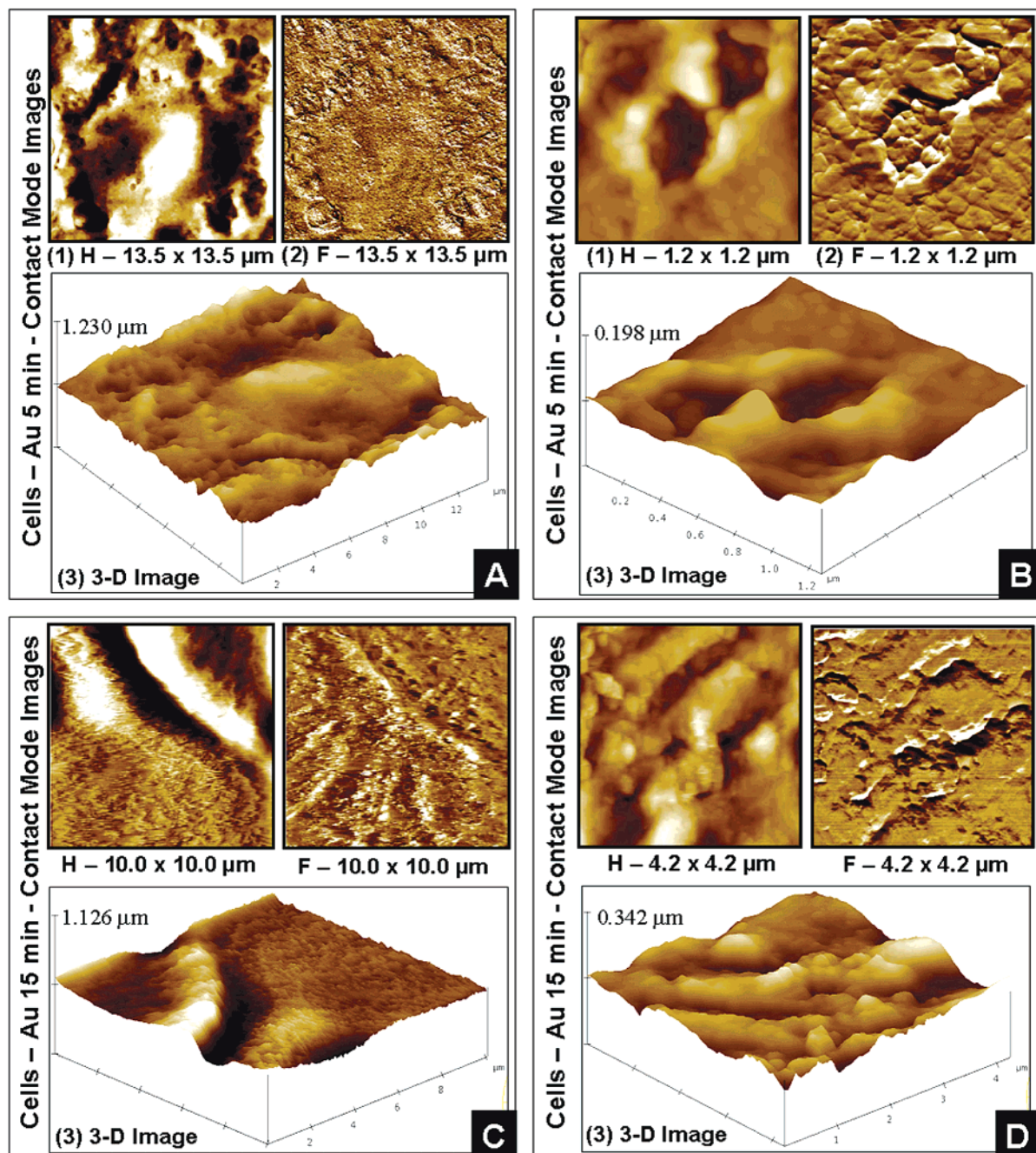


Figure 4. Contact mode AFM images of RAW264.7 macrophage cells obtained after 5 min of gold nanoparticle treatment (A and B) and after pulse-chase gold nanoparticle treatment for 15 min overnight (C and D). The notations H and F correspond to height (image 1) and friction (image 2) images, respectively. Images 3 in A–D are the 3D images of the height images shown in respective panels. All images were taken in air.

nanoparticles for 5 min. Figure 4A shows a well-defined nucleus in the center of the images (clearly visible in the 3D view in panel 3 in Figure 4A as a domelike structure) with a few micropits (depth of 25–70 nm). The nucleus is surrounded by a large number of micropits (depth of 150–300 nm) on the rest of the cell surface. Figure 4B shows higher magnification images of one of the micropits close to the nucleus (Figure 4A). The depth of the micropit shown in Figure 4B corresponds to 230 nm. The cellular domains present on the cell surface, clearly visible in panel 2 in Figure 4B, were found to be of dimensions ca. 300 nm, and the gold nanoparticle aggregates present in the micropit shown in the same figure were found to be ca. 85 nm in size. It has been reported that pinocytosis occurs for particles smaller than 100 nm and phagocytosis occurs for particles larger than 100.^{52,53} Because the gold nano-

particle used in this study ranges in size from 3 to 8 nm, involvement of the pinocytotic mechanism in gold nanoparticle uptake appears to be operative. Raynal and co-workers have recently shown the uptake of superparamagnetic nanoparticles smaller than 100 nm via pinocytosis.^{41a} Moreover, the shape of the micropits in Figure 4A also suggests gold nanoparticle uptake via pinocytosis.⁵³

Endocytosis is a vital process for macrophage cells, which leads to changes in surface and cytoskeletal architecture of the cells. After the endocytotic process of

(52) Kruth, H. S.; Jones, N. L.; Huang, W.; Zhao, B.; Ishii, I.; Chang, J.; Combs, C. A.; Malide, D.; Zhang, W. Y. *J. Biol. Chem.* **2005**, 280, 2352.

(53) Ferencik, M. *Handbook of Immunochemistry: Phagocytosis*; Chapman and Hall: London, U.K., 1993; p 387.

gold nanoparticle uptake was visualized, the logical succeeding step is to visualize the response of the cells in terms of regaining the original cell-surface architecture. To achieve this, a pulsed gold nanoparticle treatment was given to the macrophage cells for 15 min, followed by an overnight chase in nanoparticle-free media. Parts C and D of Figure 4 show the contact mode height and friction images of the cells pulsed with 50 μ M gold nanoparticles for 15 min followed by overnight chase. Both the height and friction mode images show a well-defined nucleus along with the intact membrane. The interesting point is the absence of micro- and nanopores that are clearly observed immediately after nanoparticle treatment (parts A and B of Figure 4). Indeed, the images recorded after the overnight chase are on a gross level, rather similar to the images obtained from the cells prior to gold exposure (parts A and B of Figure 3). However, some effects of the exposure of the macrophage cells to the gold nanoparticles can be discerned in the higher magnification image of the cell membrane after pulse-chase gold nanoparticle treatment (Figure 4D). Cell-surface structures appear to be generated by reconstitution of the micropits formed during the initial stages of endocytosis after gold nanoparticle treatment (panel 2 in Figure 4D).

CFLSM is one of the most important cellular analysis techniques and has been used with considerable success in the real-time observation of cells. In this technique, molecular fluorescent probes are employed to label the cells to be observed. FITC is a versatile agent used for cell imaging by confocal microscopy.⁵⁴ After observing the initial steps of endocytosis by AFM (Figures 3 and 4), confocal microscopy was used to study the kinetics of gold nanoparticle uptake at later stages of endocytosis. RAW264.7 macrophage cells treated with 50 μ M Au-lys-FITC for 30 min and 3 h were observed by CFLSM. Untreated cells were taken as a control (data not shown for reasons of brevity). Parts A and B of Figure 5 show the confocal images of the cells obtained after treatment with gold nanoparticles for 30 min; Panels A1–A3 in Figure 5 show the fluorescent image, phase image, and fluorescent image overlapped with the phase image of the cells, respectively. The gold nanoaggregates can be clearly observed as green dots in the fluorescence image (Figure 5A1) and as high contrast particle aggregates in the phase image (Figure 5A2). The overlapped image of the panels A1 and A2 in Figure 5 shown in Figure 5A3 suggests that these high contrast particles are gold nanoaggregates. Figure 5A4 shows a lower magnification image of the structures shown in panels A1–A3 in Figure 5, clearly showing the complete macrophage cell with endocytosed gold nanoparticles. Lysosomes are the organelles in the general endocytosis pathway in which endocytosed particles enter and their fate is decided. We therefore used lysotracker (a lysosome-staining red fluorescent dye) to stain the lysosomes, and then, the subcellular localization of gold nanoparticles was traced using Au-lys-FITC. Figure 5B shows the images obtained by CFLSM after treatment of RAW264.7 macrophage cells with red lysotracker as well as green-fluorescing gold nanoparticles. Panels B1 and B2 of Figure 5 show the cells, observed after sequential scanning at 543 and 488 nm, respectively. When excited using the 543 nm laser, only the lysosomes are visible in the cells as red dots (Figure 5B1), while excitation by the 488 nm argon laser enables visualization of the gold nanoparticles in the cells as green dots (Figure 5B2). Figure 5B3 corresponds to the phase-contrast image of

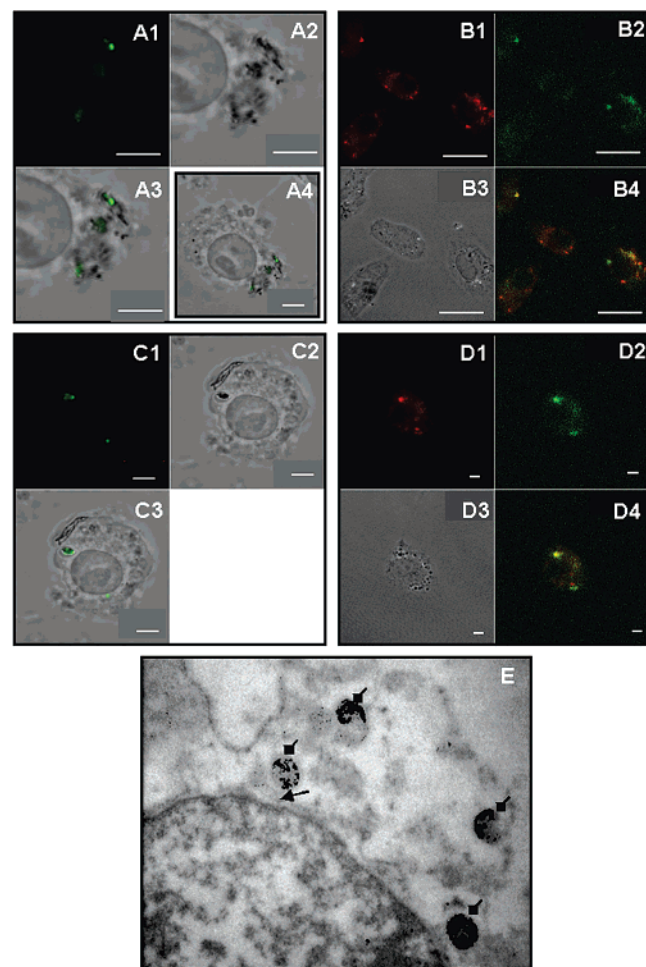


Figure 5. Confocal microscopy and TEM images of RAW264.7 macrophage cells. (A–D) CFLSM images obtained after 30 min (A and B) and 3 h (C and D) of Au-lys-FITC treatment. A and C show the images taken using only fluorescent gold nanoparticles, while B and D show the images of internalized gold nanoparticles after lysosome staining. A1–A3 and C1–C3 show the fluorescent image, phase image, and fluorescent image overlapped with the phase image of the cells obtained after gold treatment for 30 min and 3 h, respectively. A4 shows a low magnification image of the cell shown in A1–A3. B1–B4 and D1–D4 show the lysotracker captured fluorescent image, FITC captured fluorescent image, phase image, and both lysotracker and FITC fluorescent image overlapped with the phase image of the cells obtained after gold nanoparticle treatment for 30 min and 3 h, respectively. E shows the TEM image of a cell, wherein the triangle-tipped arrow identifies a reticuloendothelial network emerging out from a nuclear pore, while the square-tipped arrows show lysosomal bodies filled with gold nanoparticle aggregates. The scale bar in the CFLSM images corresponds to 5 μ m.

the cells, showing the surface topology with a well-defined nucleus. Figure 5B4 is the image obtained by overlaying panels B1–B3 in Figure 5. It is clearly evident from Figure 5B4 that the gold nanoaggregates are getting colocalized in the lysosomal bodies.

Parts C and D of Figure 5 correspond to confocal images of the cells after a 3 h treatment with fluorescent gold nanoparticles and fluorescent gold nanoparticles along with lysotracker, respectively. The images obtained in parts C and D of Figure 5 are similar to those obtained in parts A and B of Figure 5, respectively, except for the fact that, after a prolonged reaction of the macrophage cells with gold nanoparticles, the fluorescence from FITC-capped gold nanoaggregates and the lysotracker is observed closer to the nucleus. We note that no fluorescence

from the nanoparticles could be observed inside the nucleus even after prolonged exposure to the cells. The confocal microscopy analysis (parts A–D of Figure 5) thus provides compelling evidence for cellular uptake of the gold nanoparticles, their internalization in lysosomes, and time-dependent movement of these lysosomal bodies toward the nucleus before their final perinuclear arrangement; the gold nanoparticles do not enter the nucleus. However, negatively charged silica nanoparticles have recently been shown to enter inside the nucleus of the cells.^{41b} Therefore, endocytosis of various nanoparticles cannot be generalized.

To investigate whether the gold nanoparticle uptake is a temperature-dependent process, RAW264.7 cells were cultured with fluorescent gold nanoparticles under cold conditions (4 °C). We assume that this uptake would be inhibited at lower temperatures, if it were performed via endocytotic pathways. As expected, we could not observe any fluorescent gold nanoparticles inside the cells. In addition, after re-incubating the previously cooled cells at 37 °C with gold nanoparticles, their uptake by the cells studied by confocal microscopy was found to be quite facile (data not shown for brevity). These results clearly show that the uptake of gold nanoparticles in macrophage cells occurs by an endocytotic pathway. Furthermore, the presence of fluorescent gold nanoparticles selectively in endosomes/lysosomes highlights the potential use of FITC-functionalized gold nanoparticles as biocompatible endosome/lysosome markers that function without activating or disrupting cell functions. This seems to be an advantage over semiconductor quantum dots^{32,33} that are commonly used as endosome/phagosome markers⁵⁵ that have been shown to disrupt cellular function as a consequence of their cytotoxic nature.

The findings based on the AFM and CFLSM analysis were correlated with TEM of the cells after cryotomy. TEM image of a cryotomed RAW264.7 macrophage cell treated with gold nanoparticles for 24 h is shown in Figure 5E. A part of the well-defined nucleus is visible toward the lower left end of the image. The presence of an intact nuclear membrane and other membrane structures strongly suggests that the cell is viable and metabolically active. Gold nanoaggregates are clearly visible as higher contrast regions inside the lysosomes (dark patches identified by square-tipped arrows), while a few gold nanoparticle aggregates are observed outside other membrane structures. Among the various images, we could image a lysosome containing gold nanoaggregates lying immediately outside the nuclear pore (identified by a triangle-tipped arrow in Figure 5E) documenting its exact fate. The reticuloendothelial network in the form of endoplasmic reticulum can also be clearly seen emerging out from the nuclear pore, and a few gold nanoparticle aggregates are visible in this reticuloendothelial network. Perinuclear arrangement of lysosomes is also clearly established by TEM and supports the AFM and confocal microscopy findings discussed earlier on the perinuclear arrangement of lysosomes containing gold nanoaggregates.

It is interesting to note that even after 24 h of gold nanoparticle treatment, all of the lysosomes containing gold nanoaggregates are observed only around the nucleus and not dispersed in the cytosol. The next obvious question

is what happens to the gold nanoparticles once they are internalized in perinuclearly arranged lysosomes. (Are they retained inside the cells forever?) It is well-known that antigenic proteins delivered to lysosomes via endocytosis are degraded to peptides, which are then recycled to endosomes containing recycling cell-surface receptors, where they are associated with MHC class II molecules and their further processing takes place.⁵⁶ Gold nanoparticles might interfere with lysosomal enzymes involved in antigen processing because of their long-term accumulation in lysosomes, or they may directly alter MHC molecules along the lysosome–endosome pathway; hence, these mechanisms could result in reduced production and presentation of self-peptides (arthritogens). If these activities take place in conjunction with a redox system within phagocytic cells, as is suggested in this study by the reduction of RNS and ROS levels during prolonged and high gold nanoparticle concentration exposure (parts B–D of Figure 2), the anti-inflammatory action of gold can be effective over a prolonged period of time and thus of considerable value against autoimmune disorders. It is unlikely that the gold nanoparticles would be easily digested by lysosomal enzymes, and therefore, the exocytosis of gold nanoparticles is not clear at this stage and could lead to bioaccumulation of gold nanoparticles inside the cellular compartments. Issues related to the clearance mechanism of gold nanoparticles from the cells are extremely important and will be addressed in future communications.

In conclusion, we have presented detailed studies on the interaction of gold nanoparticles with phagocytes and have demonstrated the biocompatible properties of gold nanoparticles such as nontoxicity, nonimmunogenicity, and high tissue permeability without hampering cell functionality. In addition, we have shown the antioxidant effect of gold nanoparticles and the path of their eventual internalization in perinuclearly arranged lysosomes. These findings have implications in the design of effective targeted drug/gene delivery systems. The biocompatible fluorescent system employed as beacons for the nanoparticles in the present study is promising for combining cancer imaging and tumor-targeted drug delivery in cancer therapy. We believe that our initiatives in the direction of studying inherent cellular biochemical and immunological processes such as endocytosis using novel nanomaterials such as gold and nanotechniques such as AFM would provide new dimensions to the field of nanoimmunology, nanomedicine, and nanobiotechnology.

Acknowledgment. R. S. and V. B. thank the Department of Biotechnology (DBT) and Council of Scientific and Industrial Research (CSIR), Government of India, respectively, for research fellowships. We acknowledge Ms. Ashwini Atre and Ms. Hemangini Shikhare of the National Centre for Cell Sciences, Pune, for assistance with confocal microscopy and flow cytometry measurements, respectively.

Supporting Information Available: Quantitative estimation of binding of FITC to variously functionalized gold nanoparticles by fluorescence emission spectroscopy (Figure S1). SDS–PAGE image showing cellular proteins before and after exposure to 100 μ M gold nanoparticles for 24 h (Figure S2). This material is available free of charge via the Internet at <http://pubs.acs.org>.

LA0513712

(56) Germain, R. N. *Cell* **1994**, 76, 287.

(55) Hanaki, K.; Momo, A.; Oku, T.; Komoto, A.; Maenosono, S.; Yamaguchi, Y.; Yamamoto, K. *Biochem. Biophys. Res. Commun.* **2003**, 302, 496.